Two-port network modeling
for bio-heat transfers in lungs

Jean-François Duhé [*] **Stéphane Victor** [*] **Pierre Melchior** [*]
Youssef Abdelmounen [**,***] **François Roubertie** [**,***]

[*] *Univ. Bordeaux, CNRS, IMS-UMR 5218, Bordeaux INP/enseirb-matmeca, 351 cours de la Libération,*
33405 Talence Cedex France
(e-mails: name.lastname@ims-bordeaux.fr)
[**] *IHU Liryc, Electrophysiology and Heart Modeling Institute,*
Fondation Bordeaux Université 33000 Bordeaux Cedex France
[***] *INSERM, Centre de recherche Cardio-Thoracique de Bordeaux,*
33000 Bordeaux Cedex France (e-mails: name.lastname@u-bordeaux.fr)

Abstract: In open-heart surgery, temperature changes may severely damage organ tissues, therefore a better knowledge of thermal transient effects is required to improve temperature control. Heat transfer in a biological context is usually treated by means of empirical relationships or simple resistance models. In some cases, fairly simplified models only involving thermal resistance R and a heat capacity C are used. More advanced models which may be accurate enough tend to rely on heavy finite element computations. An intermediate model is sought to more accurately describe transient effects. By combining the well-known Pennes' bio-heat equation combined to a thermal two-port network, a circuit model is proposed to take into account thermal transients in a perfused tissue. A larger frequency band can be taken into account for such an approach. The proposed models may also consider the effect of blood perfusion on the temperature transients, as well as blood temperature fluctuations (as in extracorporeal circulation, for example) and metabolic heat generation. For a simple 1D scenario, sensitivities to different heat or temperature inputs are compared. The obtained impedance expressions are also analyzed for different branch levels of the lung.

1. INTRODUCTION

In medicine, temperature fluctuations have a fairly narrow variation window as even moderate temperature changes may severely damage tissues. In normal conditions, the organs of a human being remain pretty close to the body's core temperature, usually taken as $37°C$. However, in open-heart surgery, the organs are exposed to the ambiant air. Heat losses occur and the exposed organ temperature decreases. Often, thermal pads and artificial warming of the perfused tissue are applied to compensate for the heat losses. This technique being empirical, a better knowledge of thermal transient effects is required to improve temperature control for such scenarios.

Lungs are of particular interest for surgeons, as extracorporeal circulation (ECC) is normally mandatory for cardiac surgery. Under such conditions, lungs are exposed to harsh conditions and may suffer irreversible damages (see Badenes et al. (2015)). Research regarding lung protection have been carried out during such procedures (see Luo et al. (2017)). Controlling tissue temperature plays a crucial role in surgery scenarios and precise hypothermia (see Giesinger and McNamara (2018)) will protect the lungs by lowering its metabolic rate. A better understanding of temperature transients in lungs may lead to a better

control of thermal protection during ECC. Lungs have been modelled by taking multiple approaches. A bifurcating flow model (see Kuwahara et al. (2009)) proved that total lung levels (23) are an optimal point for airway resistance. An equivalent mechanical impedance approach may be simple enough to be identified in an experiment. This approach was explored in Ionescu et al. (2014), where lung fractality were introduced by using fractional-order operators. It can be shown that such models may reveal a particular illness, as lung geometric anomalies heavily change its mechanical impedance (see Copot et al. (2017)). A black-box fractional-order model based on the Havriliak-Negami function was also used in experiments to analyze effects of ECC on lung temperature distribution (Victor et al. (2020)). A powerful tool to analyze heat transfer is the use of thermal two-port networks (see Maillet et al. (2000)). By using the heat flow, $\dot{Q}$, and temperature, T, as an analogy to current and voltage, an accurate circuit model may be obtained by starting with the heat equation. The thermal system is then represented as a T circuit with series impedance $Z_1(s)$ and $Z_2(s)$ as well as a shunt impedance $Z_3(s)$ (see figure 2). Note that these impedances expressed in the Laplace domain are complex.

The thermal diffusion on a isolated semi-infinite rod is proven to have a thermal impedance in high frequency equivalent to a half-order integrator (Malti et al. (2009)):

$$Z_{thermal}(s) = \frac{T(s)}{\phi(s)} = \frac{K}{\sqrt{s}}. \qquad (1)$$

This result lead to the use of fractance elements (see Krishna (2011) and Nakagawa and Sorimachi (1992)) for thermal circuit modeling. It can be found in the literature that such elements may be used to model highly irregular systems, such as porous films in an electrochemical context (Das et al. (2009)), intestine tissue (Elwakil (2010)), and elasticity of cardiac tissue (Magin and Ovadia (2006)) which proves the interest of fractional order models for diffusive phenomena as well as complex geometries.

In living tissue, additional phenomena are not taken into account in the classic heat equation. Indeed, blood circulation allows nutrient and gas exchanges to allow organic functionalities, but this flow also acts as a natural thermal regulator. Also, cell breathing and internal processes related to metabolism may also generate heat. Pennes (1948) developed a bio-heat equation to take into account such phenomena by completing the heat equation as:

$$\rho c \frac{\partial T}{\partial t} = k \nabla^2 T + \rho_b c_b \omega_b (T_a - T) + q_m + q_{ext} \qquad (2)$$

where T_a is the arterial temperature, $\rho_b c_b \omega_b (T_a - T)$ is the perfusion term, q_m is the metabolic heat generation and q_{ext} is an external heat source.

Pennes equation remains largely used in the medical community: for global modeling of the human body (Fiala et al. (1999)), for modeling a human eye with radiative heat loss (Ooi et al. (2007)), for modeling the temperature transient in human skin (see Ratovoson et al. (2010) and Strakowska et al. (2015)), etc.

The main contribution of the present work is to provide an accurate circuit model from the bio-heat equation by applying the thermal two-port network formalism. Moreover, the impedances are expressed in all branch levels of the lungs. An analysis of the resulting impedance expressions is provided for frequency and perfusion variations, as well as identification of some main parameters. This method is also extended to include perfusion fluid temperature variations and metabolic heat generation.

Section 2 of the paper presents the bio-heat two-port network formalism. An application to impedance expressions as well as simulations of frequency response for bronchioles are presented in Section 3. Finally, conclusions and perspectives are presented in Section 4.

2. BIO-HEAT TWO-PORT NETWORK FORMALISM

The analyzed scenario is a simple plane wall of tissue that has longitudinal heat transfer along x axis as shown in figure 1. The tissue has total length L and a cross section S_w. This plane wall has thermal conductivity k, density ρ and heat capacity c. There is a perfusion fluid with density ρ_b and heat capacity c_b. Perfusion coefficient ω_b indicates the total ratio between perfusion fluid volume flow rate $\dot{V}_b$ and the total volume of the perfused tissue V_t:

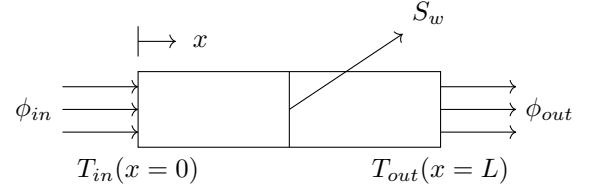$$\omega_b = \frac{\dot{V}_b}{V_t}. \qquad (3)$$

Fig. 1. 1D bio-heat thermal system

If one considers a scenario without external heat source and the influence of metabolic heat generation is negligible, equation (2) becomes:

$$\rho c \frac{\partial T}{\partial t} = k \frac{\partial^2 T}{\partial x^2} + \rho_b c_b \omega_b (T_a - T). \qquad (4)$$

In a medical context, an internal organ temperature can be considered at a constant core temperature T_b, close to the human body, namely $37°C$. By introducing the temperature variations of a tissue around the core temperature:

$$\tilde{T} = T - T_b, \qquad (5)$$

as T_b is assumed constant, the time and space partial derivatives for $\tilde{T}$ and T are equivalent. Also, under normal conditions, the arterial blood temperature T_a tends to the core temperature close to the core:

$$T_a \approx T_b. \qquad (6)$$

Consequently, relation (4) comes down to:

$$\rho c \frac{\partial \tilde{T}}{\partial t} = k \frac{\partial^2 \tilde{T}}{\partial x^2} - \rho_b c_b \omega_b \tilde{T}. \qquad (7)$$

By defining thermal diffusivity α and a perfusion heat coefficient h_b as:

$$\alpha = \frac{k}{\rho c}, \quad h_b = \frac{\rho_b c_b \omega_b}{k}, \qquad (8)$$

equation (7) becomes:

$$\frac{1}{\alpha} \frac{\partial \tilde{T}}{\partial t} = \frac{\partial^2 \tilde{T}}{\partial x^2} - h_b \tilde{T}, \qquad (9)$$

or else, by taking the Laplace transform and assuming null initial conditions, one gets:

$$\left[\frac{s}{\alpha} + h_b \right] \tilde{T}(x, s) = \frac{d^2 \tilde{T}(x, s)}{dx^2}. \qquad (10)$$

By considering a heat input $\dot{Q}_{in}$ at $x = 0$ and an output $\dot{Q}_{out}$ at $x = L$:

$$\dot{Q}_{in}(s) = -k S_w \frac{\partial \tilde{T}(x, s)}{\partial x} \bigg|_{x=0}$$

$$\dot{Q}_{out}(s) = -k S_w \frac{\partial T(x, s)}{\partial x} \bigg|_{x=L}, \qquad (11)$$

and by introducing the input temperature $T_{in} = \tilde{T}(0, s)$ at $x = 0$ and an output temperature $T_{out} = \tilde{T}(L, s)$ at $x = L$, the bio-heat equation (10) can be rewritten as a two-port network (see (Maillet et al., 2000, chap. 3)):

$$\begin{bmatrix} T_{in}(s) \\ \dot{Q}_{in}(s) \end{bmatrix} = M \begin{bmatrix} T_{out}(s) \\ \dot{Q}_{out}(s) \end{bmatrix} \qquad (12)$$

where M results from the solving of the bio-heat equation in a finite section of length L:

$$M = \begin{bmatrix} \cosh(\delta L) & \frac{1}{k S_w \delta} \sinh(\delta L) \\ k S_w \delta \sinh(\delta L) & \cosh(\delta L) \end{bmatrix} \qquad (13)$$
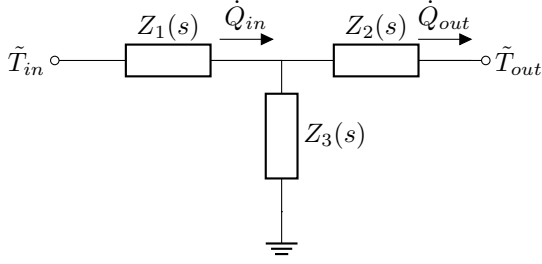
Fig. 2. Thermal two-port network

with $\delta = \sqrt{\frac{s}{\alpha} + h_b}$. Relation (12) can be represented by an equivalent T circuit model, such as represented in figure 2 (see Maillet et al. (2000)).

The expressions for the impedances are given by:

$$Z_1(s) = Z_2(s) = \frac{1}{kS_w\delta}[\coth(\delta L) - \operatorname{csch}(\delta L)] \qquad (14)$$

and

$$Z_3(s) = \frac{1}{kS_w\delta}\operatorname{csch}(\delta L). \qquad (15)$$

2.1 Series impedance Z_1 and Z_2 asymptotic behavior

In low frequency, the series impedance Z_1 (and therefore Z_2) will tend to:

$$\lim_{\omega \to 0} Z_1(j\omega) = \frac{\coth(\sqrt{h_b}L) - \operatorname{csch}(\sqrt{h_b}L)}{kS_w\sqrt{h_b}} = R_{1-bio}, \qquad (16)$$

an expression that characterizes a resistance.

Recalling the Taylor expansion at $y = 0$ and order 1 of

$$\coth(y) = \frac{1}{y} + \frac{1}{3}y + O(y^2),$$

$$\operatorname{csch}(y) = \frac{1}{y} - \frac{1}{3}y + O(y^2),$$

a low perfusion allows expressing the resistance limit:

$$\lim_{h_b \to 0} R_{1-bio} = \frac{L}{2kS_w}, \qquad (17)$$

and as perfusion becomes more significant, knowing that

$$\coth(\sqrt{h_b}L) - \operatorname{csch}(\sqrt{h_b}L) \approx 1, \text{ when } \sqrt{h_b}L > 3.5 \quad (18)$$

the resistance tends to the following limit:

$$R_{1-bio} \approx \frac{1}{kS_w\sqrt{h_b}}. \qquad (19)$$

This latter result signifies that perfusion reduces the static gain of the series impedances Z_1 and Z_2.

In high frequency, the series impedance Z_1 (and therefore Z_2) will tend to:

$$\lim_{\omega \to \infty} |Z_1(j\omega)| = 0, \quad \lim_{\omega \to \infty} \arg |Z_1(j\omega)| = -45°, \qquad (20)$$

an expression that characterizes a constant-phase element:

$$Z_{1-HF}(s) = \frac{1}{C_s\sqrt{s}} \qquad (21)$$

with $C_s = \frac{kS_w}{\sqrt{\alpha}}$.

2.2 Shunt impedance Z_3 asymptotic behavior

In low frequency, the shunt impedance Z_3 will tend to:

$$\lim_{\omega \to 0} Z_3(j\omega) = \frac{\operatorname{csch}(\sqrt{h_b}L)}{kS_w\sqrt{h_b}} = R_{3-bio}, \qquad (22)$$

an expression that also characterizes a resistance.

This result shows that a bio-heat two-port network leads to a completely resistive network in low frequency instead of the classic RC model. For a case of heat insulation at the output, a constant temperature variation $\tilde{T}_{in}$ will lead to a steady but inferior temperature variation at the output. This is logical as in this model one considers that blood flow is continuously evacuating heat all along the tissue.

A low perfusion allows expressing the resistance limit

$$\lim_{h_b \to 0} R_{3-bio} = \infty \qquad (23)$$

and as perfusion becomes more significant,

$$\lim_{h_b \to \infty} R_{3-bio} = 0. \qquad (24)$$

These limits are coherent with a non-perfused model, as Z_3 in such a case would be a pure capacitance, which behaves as an infinite impedance at low frequencies. The high perfusion limit reveals that even for really slow temperature fluctuations, a strong blood flow will block the propagation of a temperature variation input through the whole length of the tissue.

In high frequency, the shunt impedance Z_3 will tend to:

$$\lim_{\omega \to \infty} |Z_3(j\omega)| = 0, \quad \lim_{\omega \to \infty} \arg |Z_3(j\omega)| = -\infty. \qquad (25)$$

2.3 Blood temperature fluctuation and metabolic heat

On the previous subsections, a circuit model was proposed without metabolic heat generation nor external heat sources. An additional assumption was that perfusion tissue temperature was taken as $T_a = T_b$.

In a realistic scenario, there may be blood temperature variations during surgery. The perfusion fluid is usually controlled and can be set at a higher temperature than the core temperature T_b in order to compensate for high heat losses in open-heart surgery. Consequently, the perfusion fluid temperature can be defined as:

$$T_a = T_b + \Delta T_a(t), \qquad (26)$$

where T_b is the core temperature and $\Delta T_a(t)$ is a temperature variation.

Under blood temperature variation and metabolic heat generation, equation (9) then becomes:

$$\frac{1}{a}\frac{\partial \tilde{T}}{\partial t} = \frac{\partial^2 \tilde{T}}{\partial x^2} - h_b\tilde{T} + h_b\Delta T_a + \frac{q_m}{k}. \qquad (27)$$

These additional terms may be interpreted as an internal heat source. The inclusion of heat sources terms has also been treated for two-port networks in Pailhes et al. (2012)). It is now proposed to extend this latter result to the bio-heat equation (see figure 3).

Let be a heat source function $g(x,t)$ defined as:

$$g(x,t) = kh_b\Delta T_a + q_m \qquad (28)$$

If ΔT_a and q_m are independent of temperature and position, this heat generation function leads to an additional heat source in the circuit model given by:

$$\dot{Q}_d(s) = \int_0^L S_w G(s)\cosh(\delta x)dx \qquad (29)$$
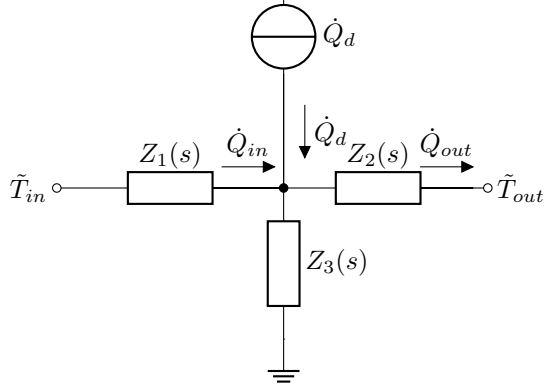
or else:

$$\dot{Q}_d(s) = G(s)F(s) \qquad (30)$$

Fig. 3. Thermal two-port network with blood temperature fluctuation and metabolic heat generation

with $G(s) = kh_b\Delta T_a(s) + q_m(s)$ and $F(s) = \frac{S_w \sinh(\delta L)}{\delta}$.

3. LUNG APPLICATION

Lungs are exposed during cardiac open-heart surgery due to ECC. As shown in previous sections, the perfusion flow rate may heavily influence thermal behavior. Thus, an adequate combination of perfusion tissue temperature ΔT_a and its flow rate (and consequently ω_b) may help to maintain the organ normal temperature during the ECC. However, lungs exhibit a fairly complex geometry as regular bifurcations appear (see figure 4).
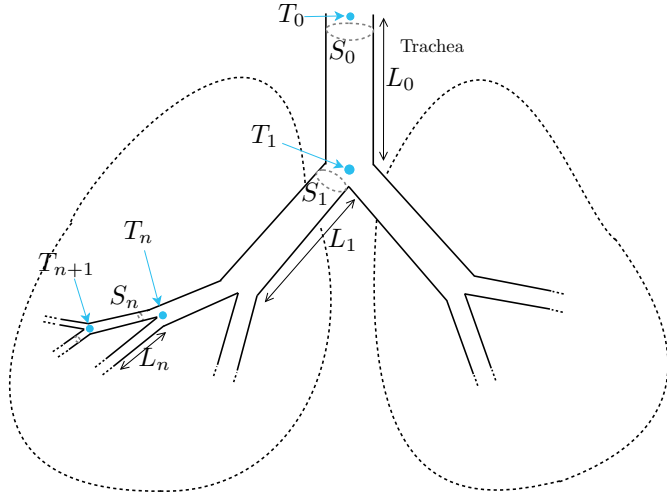

Fig. 4. Lung scheme

The complexity relies on the bifurcations when going from level n to level $n + 1$. Kuwahara et al. (2009) proposed a simplification: lung models are geometrically distributed to provide an optimal equivalent airway resistance. This means that pressure losses along these bifurcations are minimized. Thus, by applying Murray's bifurcation law, recursive relations are obtained for the diameters:

$$\frac{d_{n+1}}{d_n} = 2^{-\frac{1}{3}}, \qquad (31)$$

the cross-sections:

$$\frac{S_{n+1}}{S_n} = 2^{-\frac{2}{3}}, \qquad (32)$$

and the lengths:

$$\frac{L_{n+1}}{L_n} = 2^{-\frac{1}{3}}. \qquad (33)$$

ρ	550 $[kg][m^{-3}]$	ρ_b	1060 $[kg][m^{-3}]$
c	3718 $[J][kg^{-1}][K^{-1}]$	c_b	3900 $[J][kg^{-1}][K^{-1}]$
k	0.28 $[W][m^{-1}][K^{-1}]$	ω_b	0.0043 s^{-1}
L_0	0.1 m	d_0	1.4 cm

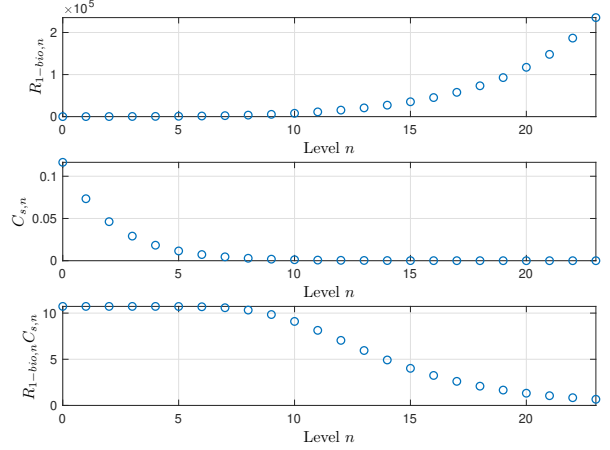Table 1. Simulation parameters for lung impedance

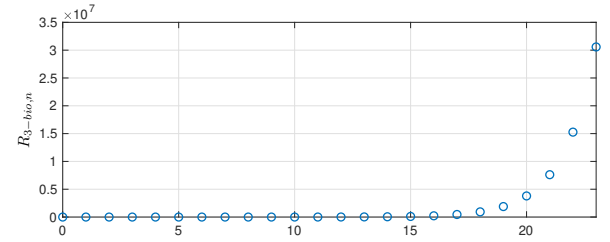Fig. 5. $R_{1-bio,n}$ and $C_{s,n}$ for multiple lung levels

Fig. 6. $R_{3-bio,n}$ for multiple lung levels

In this way, it is possible to provide the expressions of the two-port network impedances at any level n, as follows:

$$Z_{1,n}(s) = \frac{2^{\frac{2n}{3}}}{kS_0\delta}[\coth(2^{-\frac{n}{3}}L_0\delta) - \operatorname{csch}(2^{-\frac{n}{3}}L_0\delta)] \quad (34)$$

$$Z_{3,n}(s) = \frac{2^{\frac{2n}{3}}}{kS_0\delta}\operatorname{csch}(2^{-\frac{n}{3}}L_0\delta). \qquad (35)$$

3.1 Resistance and fractance evolution in the lungs

Table 1 shows the parameters used for simulations which are defined according to human body characteristics. The evolution of the key parameters such as low frequency resistances $R_{1-bio,n}$ and $R_{3-bio,n}$ as well as constant-phase parameter $C_{s,n}$ for the impedances $Z_{1,n}$ and $Z_{3,n}$ according to the branch level n are plot in figures 5 and 6.

For Z_1, by only considering low and high-frequency limits, an asymptotic impedance approximation may be obtained:

$$Z_{1-bio,n}(s) = \frac{R_{1-bio,n}}{1 + R_{1-bio,n}C_{s,n}\sqrt{s}}. \qquad (36)$$

Therefore, $R_{1-bio,n}C_{s,n}$ may be interpreted as a time constant. Figure 5 shows that resistance increases as levels approach alveoli ($n = 23$). Note that this progression is highly nonlinear, as the airways exhibit a relatively low
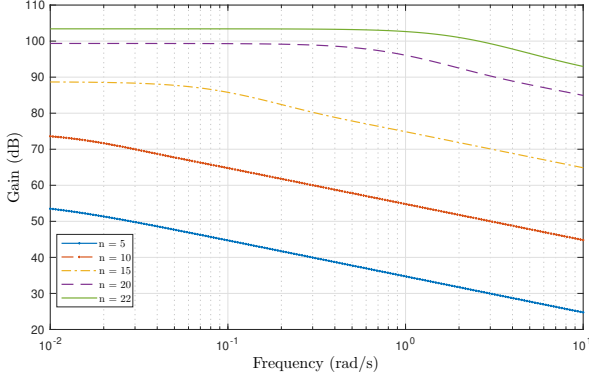
Fig. 7. $Z_{1,n}$ frequency response for different levels

Fig. 8. $Z_{3,n}$ frequency response for different levels

resistance up to $n = 10$ and then grows exponentially. Fractance $C_{s,n}$ decreases exponentially up to $n = 10$. In order to get a deeper understanding of this impedance dynamics, the time constant $R_{1-bio,n}C_{s,n}$ was also plotted. It shows that even though resistance dramatically increases after $n = 10$, fractance $C_{s,n}$ is so small that the time constant does not show a dramatic change over the whole lung. System becomes faster for smaller levels, but the progression is slower (the final and initial values have a factor of 10 between them). Note that the time constant is constant for the whole entry (up to $n = 6$).

$R_{3-bio,n}$ is low up to $n = 15$, which implies that temperature variations at the section entry are absorbed through the tissue and do not manage to significantly alter the output temperature. However, as n increases, this resistance blows up to values significantly higher than those found for $R_{1-bio,n}$: a temperature input may more easily be transmitted to the section end. As both resistances blow up for the higher levels, a global lung thermal circuit will behave approximately as an open circuit at a given level and the whole lung structure may not be required to provide an accurate thermal model. Further studies should be done to take into account the vast number of alveoli in the lungs as well as its bifurcation geometry.

3.2 Frequency responses of $Z_{1,n}$ and $Z_{3,n}$

While breathing, heat and temperature vary in time, thus frequency responses may be analyzed over a realistic frequency range. Human breathing is not a fast phenomena, but can go up to 20 breaths per minute in normal conditions. However, on most adults the breathing rate is around 12 breaths per minute. Slow breathing is considered in the range $[0.07 - 0.16]$Hz (see Russo et al. (2017)). Above 14 breaths per minute (or 0.23Hz), breathing can already be considered as an abnormal value (see Cretikos et al. (2008)). Also, the simulations will be carried out in the frequency range $[0.01 - 10]$rad/s in order to cover normal breathing. Figures 7 and 8 show the gain frequency responses for $Z_{1,n}$ and $Z_{3,n}$.

In the lung first levels, $Z_{1,n}$ behaves as a pure fractance. As one gets in deeper branches the resistance low-frequency behavior becomes more evident. The higher the level n, the smaller the branches, the higher the cut-off frequency.

For $Z_{3,n}$, low levels have extremely low gains and could almost be considered as a short circuit. This is logical as
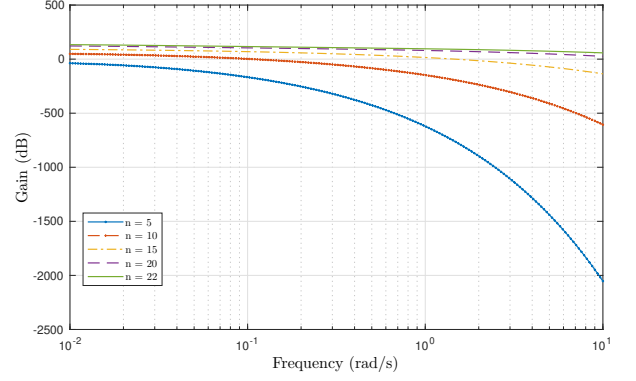
a long section will have more volume for heat evacuation. The higher the level n, the greater the static gain. On the frequency range, the low-frequency resistance behavior is not visible. On the other hand, one may notice for low frequencies in the curves for $n = 15$ and $n = 20$ that the initial slope is around -20dB/dec, which implies a capacitance behavior. As frequency increases, this slope increases, which implies further high frequency filtering.

3.3 Perfusion tissue temperature variation

A simple academic scenario is proposed to observe the system sensitivity to a variation in perfusion fluid temperature. The input will be considered to be at the body core temperature $\tilde{T}_{in} = 0$ and the output will be insulated $\dot{Q}_{out} = 0$. Therefore, the transfer function relating an output temperature deviation $\tilde{T}_{out,n}$ (at level n) and perfusion fluid variation ΔT_a will be:

$$H_{T_a,n}(s) = \frac{\tilde{T}_{out,n}(s)}{\Delta T_a(s)} = \frac{k h_b S_w \sinh(\delta L) Z_{1,n}(s) \cdot Z_{3,n}(s)}{\delta \left[Z_{1,n}(s) + Z_{3,n}(s) \right]} \tag{37}$$
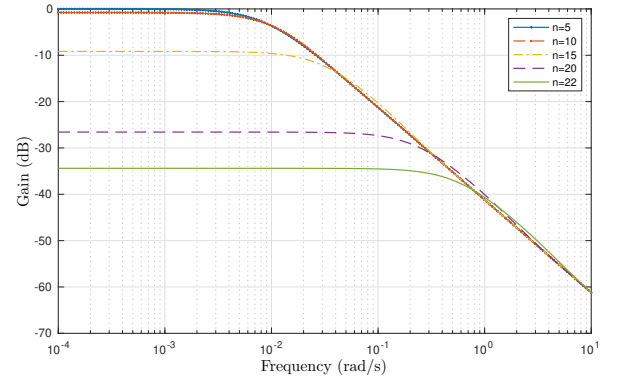

Fig. 9. $H_{T_a}(s)$ frequency response for different levels

Figure 9 shows the gain frequency response of $H_{T_a,n}$. For low levels, length difference is not significant as the static gains for $n = 5$ and $n = 10$ are almost identical. Both levels can be considered as long enough for the null input to be fully compensated by fluid temperature. For both curves, the static gain is $0\,dB$: slow fluid temperature variations will easily affect the whole system. As levels increase, static gain is reduced because of smaller dimensions. There is a clear first-order low pass filter behavior for all levels.

4. CONCLUSION AND PERSPECTIVES

A new heat transfer modeling in a perfused tissue is proposed by combining Pennes bio-heat equation and the quadrupole network: a T circuit model with impedances $Z_{1,n}$ and $Z_{3,n}$ is obtained that depends on the system geometry and thermal properties. The thermal properties of a perfusion tissue as well as its perfusion coefficient ω_b influence the impedance expressions. A theoretical analysis was carried out on the impedance frequency behaviors as well as the perfusion influence. The results are coherent and support the blood flow as a natural thermal regulation. The circuit model was modified to allow the inclusion of metabolic heat rate and perfused fluid temperature variations. Lung application showed an expected low-pass behavior for impedance and static gain evolutions as going into lung higher levels. High levels exhibit extremely high resistance suggesting open circuit behavior. Lung global geometry should also be taken into account. For perspectives, the lung successive branching could be considered to analyze if the number of alveoli is enough to compensate for its high resistance. A global lung model could be studied where dead alveolar space and exchange alveolar space are used. Perfusion coefficient may be more accurate if modelled as a function of the current level n. Finally, recursive system identification could be implemented, so that surgeons get a precise knowledge of the lung during surgery.

REFERENCES

Badenes, R., Lozano, A., and Belda, F. (2015). Postoperative pulmonary dysfunction and mechanical ventilation in cardiac surgery. *Critical Care Research and Practice*, 420513. doi:10.1155/2015/420513.

Copot, D., De Keyser, R., Derom, E., and Ionescu, C. (2017). Structural changes in the copd lung and related heterogeneity. *PLOS ONE*, 12(5). doi:10.1371/journal.pone.0177969.

Cretikos, M., Bellomo, R., Hillman, K., Chen, J., Finfer, S., and Flabouris, A. (2008). Respiratory rate: the neglected vital sign. *Medical Journal of Australia*, 188(11), 657–659. doi:10.5694/j.1326-5377.2008.tb01825.x.

Das, S., Sivaramakrishna, M., Das, S., and Biswas, K.and Goswami, B. (2009). Characterization of a fractional order element realized by dipping a capacitive type probe in polarizable medium. In *Symposium on Fractional Signals and Systems*. Lisbon, Portugal.

Elwakil, A. (2010). Fractional-order circuits and systems: An emerging interdisciplinary research area. *IEEE Circuits and Systems Magazine*, 10(4), 40–50. doi:10.1109/MCAS.2010.938637.

Fiala, D., Lomas, K., and Stohrer, M. (1999). A computer model of human thermoregulation for a wide range of environmental conditions: the passive system. *J Appl Physiol (1985)*, 87(5). doi:10.1152/jappl.1999.87.5.1957.

Giesinger, R. and McNamara, P. (2018). The Impact of Therapeutic Hypothermia on Pulmonary Hemodynamics of Meconium Aspiration Syndrome. *American Journal of Respiratory and Critical Care Medicine*, 198(2). doi:10.1164/rccm.201802-0207LE.

Ionescu, C.M., Copot, D., and De Keyser, R. (2014). A fractional order impedance model to capture the structural changes in lungs. *IFAC Proceedings Volumes*, 47(3), 5363–5368. doi:10.3182/20140824-6-ZA-1003.01124.

Krishna, B. (2011). Studies on fractional order differentiators and integrators: A survey. *Signal Processing*, 91(3), 386 – 426. doi:10.1016/j.sigpro.2010.06.022.

Kuwahara, F., Sano, Y., Liu, J., and Nakayama, A. (2009). A Porous Media Approach for Bifurcating Flow and Mass Transfer in a Human Lung. *Journal of Heat Transfer*, 131(10). doi:10.1115/1.3180699.

Luo, S., Wang, Y., An, Q., Chen, H., Zhao, J., Zhang, J., Meng, W., and Du, L. (2017). Platelets protect lung from injury induced by systemic inflammatory response. *Scientific Reports*, 7(1), 42080. doi:10.1038/srep42080.

Magin, R. and Ovadia, M. (2006). Modeling the cardiac tissue electrode interface using fractional calculus. *2nd IFAC Workshop on Fractional Differentiation and its Applications*, 39(11), 302 – 307. doi:10.3182/20060719-3-PT-4902.00056.

Maillet, D., André, S., Batsale, J., Degiovanni, A., and Moyne, C. (2000). *Thermal Quadrupoles: Solving the Heat Equation through Integral Transforms*. Loyola Symposium Series. John Wiley & Sons.

Malti, R., Sabatier, J., and Akçay, H. (2009). Thermal modeling and identification of an aluminium rod using fractional calculus. In *15th IFAC Symposium on System Identification (SYSID'2009)*, 958–963. St Malo, France. doi:10.3182/20090706-3-FR-2004.00159.

Nakagawa, M. and Sorimachi, K. (1992). Basic characteristics of a fractance device. *IEICE Transactions on Fundamentals of Electronics, Communications and Computer Sciences*, 75, 1814–1819.

Ooi, E., Ang, W., and Ng, E. (2007). Bioheat transfer in the human eye: A boundary element approach. *Engineering Analysis with Boundary Elements*, 31(6), 494–500. doi:10.1016/j.enganabound.2006.09.011.

Pailhes, J., Pradere, C., Battaglia, J., Toutain, J., Kusiak, A., Aregba, A., and Batsale, J. (2012). Thermal quadrupole method with internal heat sources. *International Journal of Thermal Sciences*, 53, 49 – 55. doi:10.1016/j.ijthermalsci.2011.10.005.

Pennes, H. (1948). Analysis of tissue and arterial blood temperatures in the resting human forearm. *Journal of Applied Physiology*, 1(2), 93–122. doi:10.1152/jappl.1948.1.2.93.

Ratovoson, D., Jourdan, F., and Huon, V. (2010). A study of heat distribution in human skin: use of infrared thermography. In *ICEM 14 – 14th International Conference on Experimental Mechanics*, volume 6, 1–8. doi:10.1051/epjconf/20100621008.

Russo, M.A., Santarelli, D.M., and O'Rourke, D. (2017). The physiological effects of slow breathing in the healthy human. *Breathe (Sheffield, England)*, 13(4), 298–309. doi:10.1183/20734735.009817.

Strakowska, M., De Mey, G., Witcek, B., and Strzelecki, M. (2015). A three layer model for the thermal impedance of the human skin: Modeling and experimental measurements. *Journal of Mechanics in Medicine and Biology*, 15(4). doi:10.1142/S021951941550044X.

Victor, S., Melchior, P., Pellet, M., and Oustaloup, A. (2020). Lung thermal transfer system identification with fractional models. *IEEE Transactions on Control Systems Technology*, 28(1), 172–182. doi:10.1109/TCST.2018.2877606.